

Assessing COMSOL Performances on Typical Electromagnetic Problems Faced by Turbo-Generator Manufacturers

E. A. Badea^{*1}, J. Oesterheld¹, S. Friedel² and M. Olsson²

¹Alstom (Switzerland) LTD, ²COMSOL AB

*Corresponding author: Zentralstrasse 40, 5242 Birr, Switzerland, eugene.badea@power.alstom.com

Abstract: Multiphysics processes manifest in turbo-generators due to the leakage electromagnetic field of the stator and rotor end winding and its associated effects at machine frontal end. Such processes are a compilation of coupled phenomena having different electromagnetic, thermal, fluid flow and mechanical backgrounds. Electric current circulation through the metallic frames used for stator core clamping and support, insulation design for the stator end winding, or electromagnetic forces acting on the stator end winding involute, are just a few relevant topics of interest for turbo-generator manufacturers. This paper presents three benchmark models, which represent the typical physical problems encountered in the turbo-generator frontal end region, and the results determined with these models simulated in COMSOL Multiphysics.

Keywords: Turbo-generator, Eddy currents, Surface electric charge, Smart thin transition layer.

1. Introduction

For turbo-generator manufacturers the Multiphysics processes due to the leakage electromagnetic field at machine end regions (see Figure 1) are of high relevance. The complex geometry, the type of materials used for different assembly modules and, the relatively strong leakage magnetic field due to the stator end winding, lead to a variety of situations, where the effects e.g. in regard of circulating currents or local overheating are hard to predict. However, such aspects must be well understood and corrections should be applied if needed to counter any undesired effects. For example, an inter-laminar insulation fault between iron sheets of the stator core due to high inter-laminar voltages or local hot-spots could lead to complex phenomenon with the potential of significant damages. Therefore the efficiency of a good numerical solver would manifest especially in understanding the causes leading to such faults,

while finding solutions for correcting them accordingly already in the design phase of a generator.

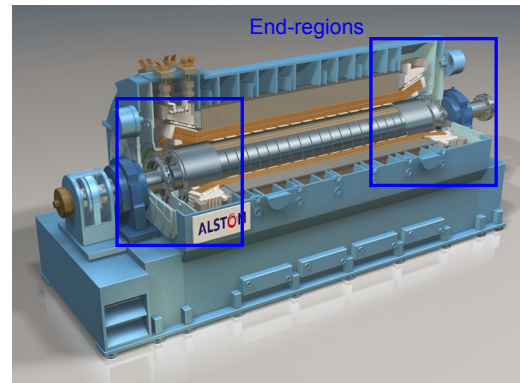


Figure 1. Turbo-Generator

The machine housing is a preferred path for such induced eddy currents produced by the leakage magnetic field, and therefore, their good modeling would deliver important input for an appropriate design of a turbo-generator. A numerically ‘badly behaving’ ferromagnetic material, characterized by high electric conductivity and high magnetic permeability, would lead to large contrasts against the surrounding air zone, where special features should be seen at work. The resulting low skin depth would drop the necessary mesh size to very small values in the housing, while the presence of the surrounding air with low conductivity and low permeability leads to a badly defined problem, where iterative solvers might not converge and direct solvers do become imperative. The nonlinear magnetic permeability dependence with respect to the local magnetic field strength would complicate the situation further. Especially for new developments with expanding requirements regarding power density a good knowledge about these parasitic effects is essential.

The same is valid for the electrical insulation system of a turbo-generator. Higher demands regarding power density necessarily lead to increased design voltages and electrical design

stresses in the stator insulation system. The term ‘stress’ in the current context, refers to the electric stress of electrically insulating materials if exposed to high electric field strengths. Whereas improved main insulation materials support this development, the critical area once more remains the end-winding region. Here the stator winding faces the same problems known from medium and high voltage cable technology, where the cylindrically-symmetric field in the solid cable insulation ends at the cable end and strong stress concentration at the end of the cable shield is to be avoided by appropriate stress grading measures. In contrast to cables, the available space in the generator end winding for stress grading measures is very limited and the field distribution is complex due to the 3-dimensional shape of the conductors and the 3-dimensional arrangement of parallel and non-parallel conductors, all operating at different potential (see Figure 2).



Figure 2. Stator end-winding of a turbo-generator

The main task of the stress grading is to protect the stator end winding against electric discharges during operation, but also during high voltage tests in the factory and on site with significantly higher voltages. Due to the limited space in the end-winding, a thin layer of strongly electrically nonlinear semiconductive material is applied on the insulated stator bar by most of the turbo-generator manufacturers. By this the originally just capacitive determined potential distribution along the surface of the insulated conductor is redistributed by an additional resistive current component in the stress grading layer. The severe nonlinearity of the stress grading material

is significantly different from a standard magnetic saturation model. If for magnetic materials the nonlinear transition zone can be considered as a buffer between the two linear states describing either full saturation or weak residual field zones, for the electrical insulation problem, the entire material is in a permanently nonlinear state. The electrical resistivity dependence with respect to electric field strength, which for example can be reproduced as a piecewise exponential set of functions, produces such a severe nonlinearity, that any tiny perturbation could lead to a chaotic uncontrolled convergence behavior of a non-appropriate solver.

Three different benchmarks were considered to validate COMSOL results against published experimental and numerical data, available in the technical literature. These benchmarks have simple geometries but include all mathematical complexities previously described, characterizing typical situations relevant in turbo-generator R&D.

2. Benchmark No. 1: Insulation Design Study

The 1st benchmark is an insulation design problem representing a simplified situation of the stator end-winding in turbo-generators. As shown in Figure 3, a thin semiconductive film applies on the main insulation for a stator winding bar leaving the stator core. The strongly electrically nonlinear semiconductive layer redistributes the mainly displacement type currents at the bar end, while grading out the electric potential along the surface. The stator end-winding can be considered as a chain of asymmetric four-poles consisting of two capacitances. With the stress grading applied, the resistances of the stress grading act in parallel to the longitudinal capacitances. Due to the relatively low currents flowing in this network, inductive type couplings are simply disregarded. The effect of the nonlinearity of the stress grading is that at points with originally high field strength the resistivity of the layer is strongly reduced, which leads to a reduced voltage gradient compared to less stressed regions. One can easily see that this situation is a clear Multiphysics problem. In regions with reduced resistivity the currents in the stress grading

increase, the losses increase and consequently the temperature increases. Knowing that the nonlinear characteristic of the stress grading material is also temperature dependent the complexity of the process becomes obvious already without adding the interference by conductors of different turns or phases. The Multiphysics problem will not be discussed in this paper.

an appropriate upper limit of the time step in order to reduce the number of nonlinear loops.

The results of the simulations were within the range of expectations, known from other FEM and discrete network simulations as well as from measurements done with the electro-optic field sensor described in [6].

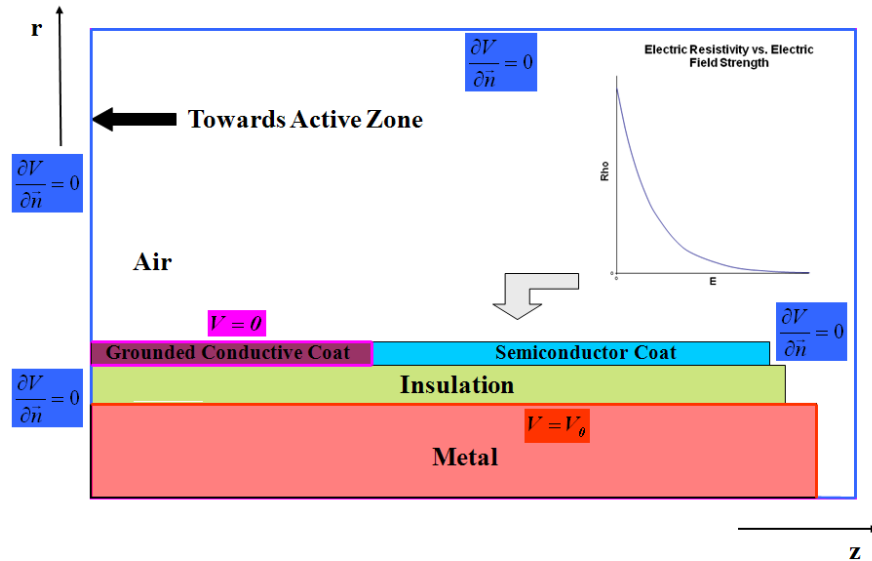


Figure 3. Benchmark No. 1 (Stress Grading): Geometry, material and boundary conditions

The basic field calculation problem is mathematically expressed in the time domain as:

$$\nabla \cdot \left(-\sigma(\vec{E})\nabla V - \varepsilon(\vec{E})\nabla \left(\frac{\partial V}{\partial t} \right) \right) = 0 \quad (1)$$

In a first approach, the model was solved in 2D using the AC/DC module running in the time domain, where the semiconductive coat was considered as a meshed domain with appropriate material properties, where the severe nonlinearity of the electrical resistivity profile with respect to local electric field strength was transferred via a parameter table to COMSOL, where it was interpolated as a continuous characteristic.

It was experienced, that due to this strong nonlinearity, tiny time steps should be used at the simulation start of a time domain simulation. The default predictor-corrector algorithm available in the COMSOL Electric Currents solver helped in this case to reduce the CPU-time, but it turned out to be advantageous to set

Figure 4 shows the axial distribution of the electrical potential and electric field strength along the surface of the stator bar without a stress grading layer. The ground electrode reflecting the end of the active part of the generator core is ending at an axial co-ordinate of 170 mm. One can see that the surface potential increases very quickly starting from this point, leading to high electrical field strength values, with the risk of destructive electrical discharges.

As shown in Figure 5, the nonlinear semiconductive coat on the surface of the bar leads to an electric potential grading along the bar end, and consequently, to an electric field strength reduction, while protecting the bar surface against electric discharges. The periodic transfer between situations where either conductive or displacement type currents in axial direction at the bar end are dominant leads to such a dynamic transient behavior, which explains the shift of peak electric field strength in both time and space.

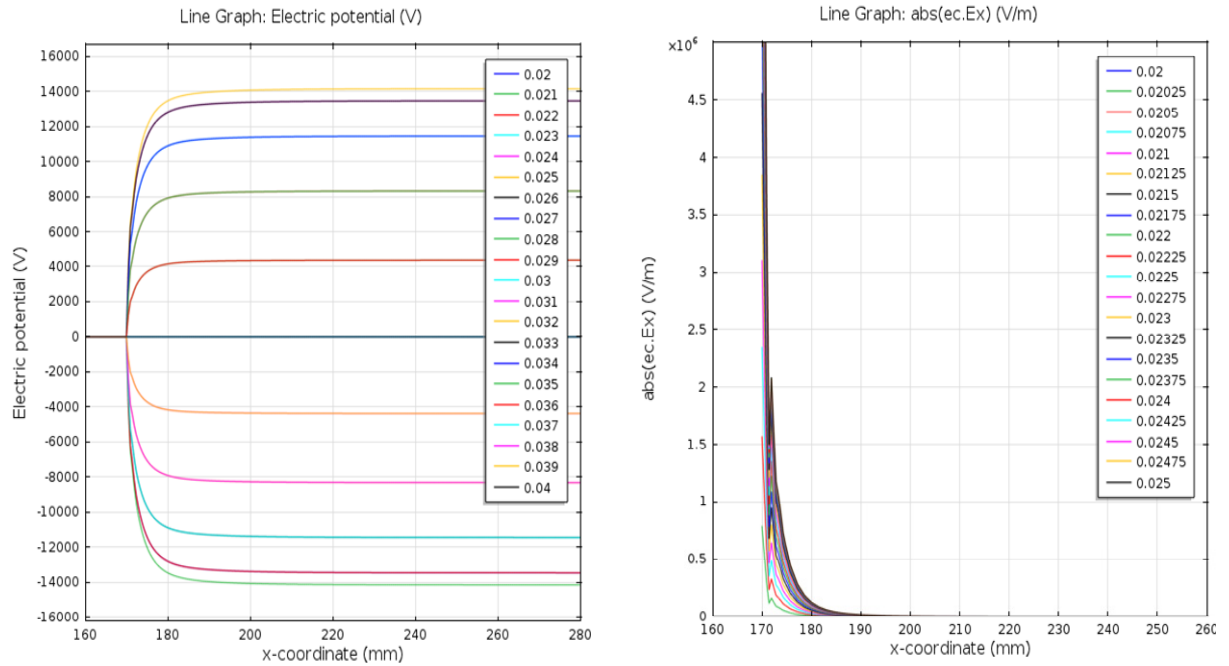


Figure 4. Stator bar end region without stress grading
 a) Potential distribution along the insulation surface at different time instants
 b) Electric field strength along the insulation surface at different time instants

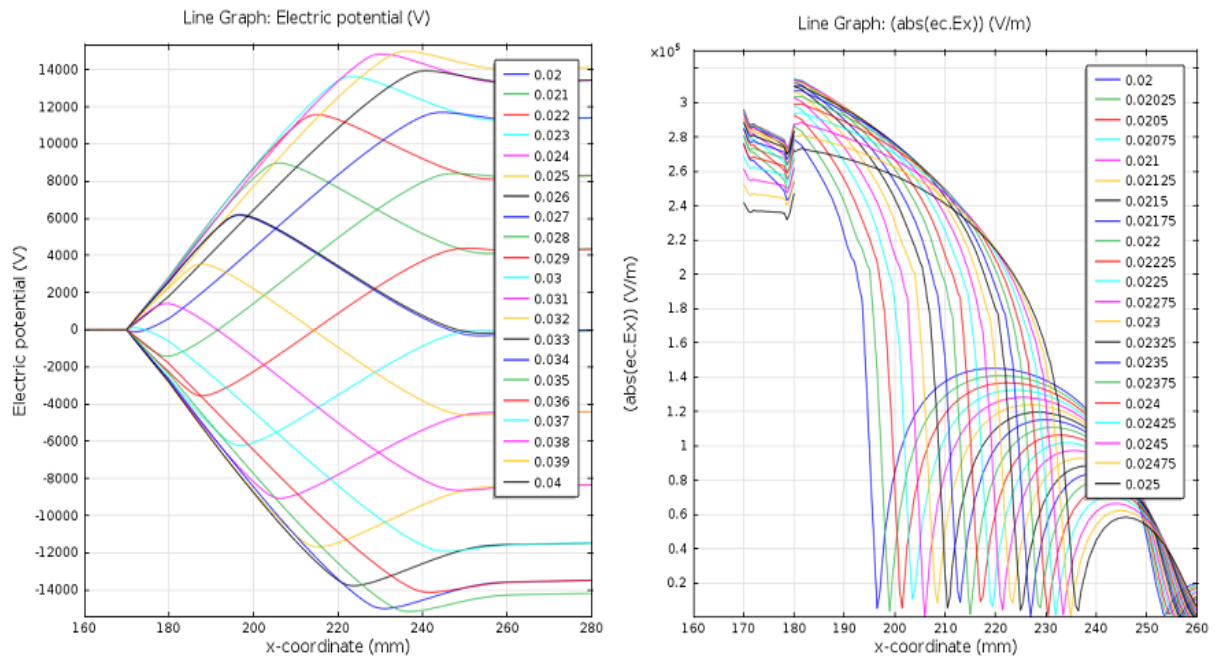


Figure 5. Stator bar end region with nonlinear field dependent stress grading
 a) Potential distribution along the insulation surface at different time instants
 b) Electric field strength along the insulation surface at different time instants

The computed electric potentials were in the expected range while their patterns matched well the profiles expected from earlier simulations and experiments.

To emphasize the benefits offered while using smart thin transition layers, the same simulation was repeated while considering the frequency domain solver and replacing the semiconductive meshed layer with a thin mixed conductive and dielectric shielding boundary condition:

$$j\omega\left(\left(\bar{\mathbf{D}}_2 - \bar{\mathbf{D}}_1\right) \cdot \bar{\mathbf{n}}\right) + \left(\sigma_1 \frac{\partial V}{\partial \bar{\mathbf{n}}} - \sigma_2 \frac{\partial V}{\partial \bar{\mathbf{n}}}\right) = \quad (2)$$

$$= -\nabla_t \cdot \left(\left(\sigma_s + j\omega\epsilon_0\epsilon_{rs}\right) d_s \nabla_t V\right)$$

where ∇_t is tangential gradient operator, while d_s , σ_s and ϵ_{rs} are the semiconductive film thickness, its electric conductivity (nonlinear, field dependent) and relative electric permittivity.

It was experienced, that the proper selection of the residual electric conductivity value for the main insulation of the stator bar was critical. A value of 10^{-12} S/m was sufficiently low to reach an accurate solution, which turned out to be comparable to the solution from the meshed, time domain model described above.

3. Benchmark No. 2: TEAM 7 – Asymmetric Conductor with a Hole

The 2nd benchmark problem was introduced at the TEAM workshop [1] and is commonly known as TEAM 7 benchmark. Induced eddy currents are computed in a thick aluminum plate having an off-centered hole, which is asymmetrically placed in the non-uniform magnetic field produced by the AC current circulating through a race-track coil. The problem geometry is shown in Figure 6 below. The problem was simulated using the AC/DC module in frequency domain. An overview on impressed currents in the coil as well as induced currents and current density in the plate is shown in Figure 7.

In order to evaluate the simulation results quantitatively, the z-component of magnetic induction along a line parallel to the plate surface in the middle between the coil and the plate was determined and compared to the corresponding results given in [2]. Furthermore, the current density of the induced eddy currents along a line

at the surface of the aluminum plate was determined and compared to the results reported in [2].

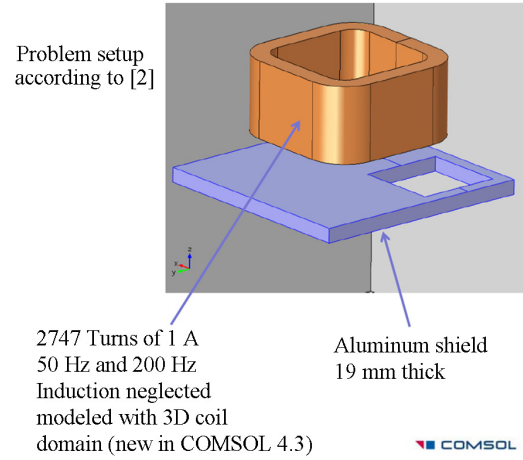


Figure 6. Benchmark No. 2 (TEAM 7): Geometry and materials

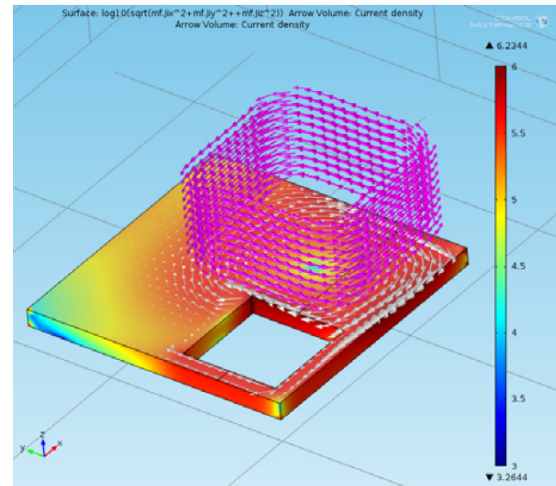


Figure 7. Benchmark No. 2: Impressed coil current (magenta) and induced currents in the aluminum plate (gray) at 50 Hz; current density in the plate represented by the surface color

Figure 8 and Figure 9 show an excellent match of the COMSOL solution to experimental data reported in [2] when comparing the magnetic induction along segment AB, and for the eddy current density along segment CD. The COMSOL solutions shown on both plots as lines are following the markers representing the experimental data collected from technical literature [2]. The match is good for both, simulations at 50 Hz and 200 Hz.

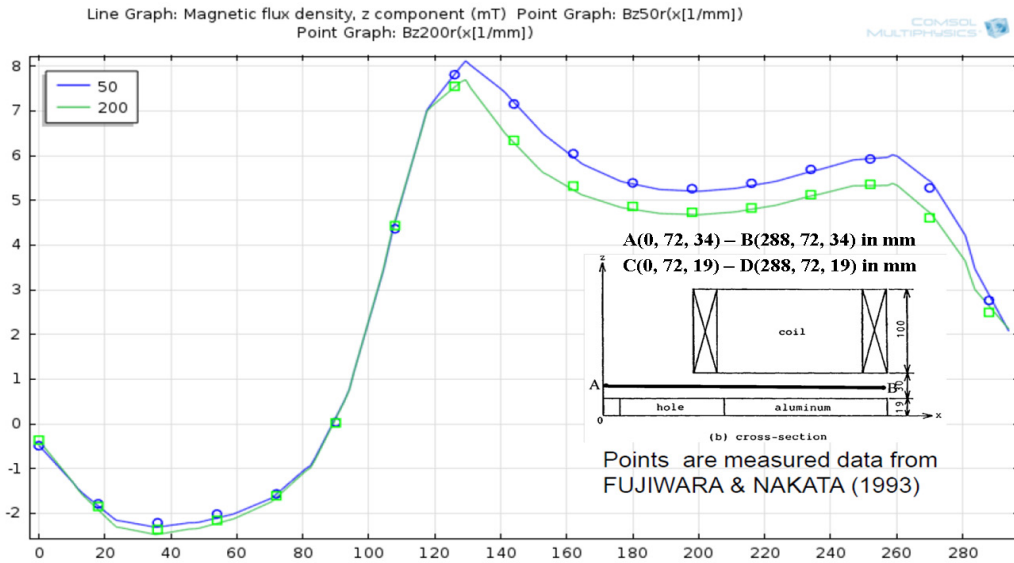


Figure 8. Benchmark No. 2:
Z-component of magnetic induction along a line AB according to [2] for 50Hz and 200 Hz;
lines represent the COMSOL results, markers represent the measured data from [2]

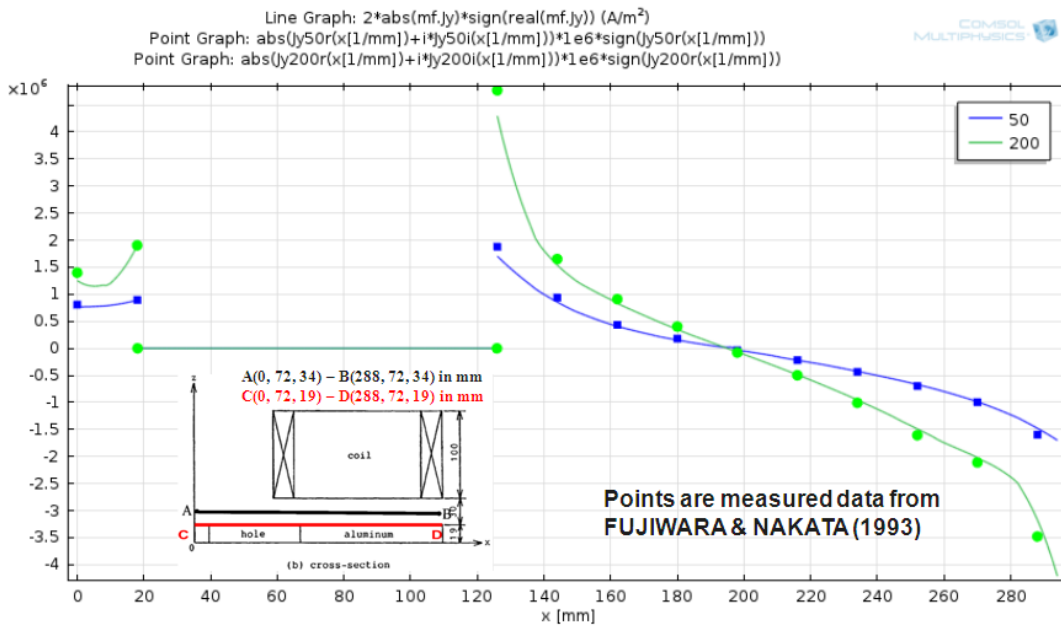


Figure 9. Benchmark No. 2:
Y-component of induced eddy current density along a line CD according to [2] for 50 Hz and 200 Hz; lines
represent the COMSOL results, markers represent the measured data from [2]

From the underlying physics, TEAM 7 remains an interesting problem because it is addressing the coupling between eddy currents produced by the time varying magnetic field, and electro-kinetic currents triggered by the electric potential variation. The (\vec{A}, V) formulation was used to solve Maxwell's equations but only in the coil domain where it really matters. Otherwise, one relied only on the \vec{A} formulation for the rest of the computational domain. The magnetic vector potential variable \vec{A} characterizing the magnetic field interacts with an electric scalar potential V , describing the Coulomb electric field strength (electro-kinetic) component. Correspondingly:

$$\nabla \times (\nu \nabla \times \vec{A}) = \vec{J}_s + \sigma \left(-\frac{\partial \vec{A}}{\partial t} - \nabla V \right) \quad (3)$$

$$\nabla \cdot \left(-\sigma \frac{\partial \vec{A}}{\partial t} - \sigma \nabla V \right) = 0 \quad (4)$$

where ν is the magnetic reluctivity, σ is the electric conductivity, and \vec{J}_s is the impressed source current density driving the electromagnetic problem.

The presence of a hole within the aluminum plate triggers a strong electric conductivity contrast between metal and surrounding air. This combined together with a non-zero normal electric field strength radiating from the plate would lead to surface electric charge build-ups on the metallic surface [3]. The electric field strength radiating from the plate would energize the air volume surrounding the metal.

Such strong electromagnetic contrast scenarios are quite common in a turbo-generator because of its laminated ferric stator core. The presence of the inter-laminar insulating layer placed in between adjacent laminations, would lead to such electric charge build-ups, which further, would trigger axial displacement currents circulating between the adjacent laminations. A fraction of the electromagnetic energy stored would be of electric type, due to the electric charge build-up at metal-inter-laminar insulation interface. The shift from a dominant magnetic to a residual electric energy stored in the stator core is due to the entanglement between conductive and displacement type currents trafficking within the ferric laminations and the inter-laminar insulation layers. Paths of 'vagabond' uncontrolled circulating currents would

correspond to local 'energized corridors' within the core, where such electric energy - magnetic energy exchanges occur. Such 'energized corridors' would have a non-uniform distribution within the stator core, and would be sensitive to any fluctuations encountered in the local magnetic state of such ferric laminations. This opens the door to a 3rd benchmark, where such interactions between induced eddy currents and electric charge build-ups are considered, while a magnetically nonlinear medium is also present.

4. Benchmark No. 3: TEAM 21 – Ferric Plate Shielded by a Copper Screen

The 3rd benchmark is known as TEAM 21, which, in addition to the previously discussed technicalities for TEAM 7, is introducing magnetic nonlinearities. Two oppositely wound, race-track coils produce a gradient magnetic field, in the vicinity of a copper screen shielding a magnetically nonlinear thin iron plate. Such a scenario would correspond to laminated end plates that are used for stator core clamping in turbo-generators. Copper shielding is used by manufacturers to screen out the plate against the leakage magnetic field of the stator end winding. The problem geometry is illustrated in Figure 10. The impressed source current and the current density distributions of the induced eddy currents in the copper and iron plates are shown in Figure 11 below.

By examining Figure 11, it can be observed how the copper plate reacts to the primary gradient magnetic field produced by the two oppositely wound solenoids. Secondary magnetic field responses of induced eddy currents circulating in the shield, would oppose the primary magnetic field. Such secondary magnetic fields would trigger tertiary type eddy current responses in iron, producing tertiary magnetic field reactions opposing the secondary ones. A reaction to a reaction event is encountered, leading to complicated current trafficking paths in the two neighboring plates, as noticed from Figure 11.

For example, if considering the primary magnetic field path produced by the 1st solenoid, the induced eddy current path in the copper shield can be constructed, since it sources out the secondary magnetic field reactions opposing the primary magnetic field. A lattice of eddy current loops would result, where induced currents

circulate in planes orthogonal to the direction of primary magnetic field. The presence of the oppositely wound 2nd solenoid, would lead to an opposing second eddy current lattice overlapping the first one. The output of such overlapping would lead to an eddy current longitudinal flow, aligning with the primary magnetic field direction, to ensure closed current loops. Such longitudinal eddy current paths due to the overlapping of the two eddy current lattices, are reaching a maximum along the transversal edges of the shield, as shown in Figure 11.

Such an event is amplified by the presence of the ferric plate, which is responding with magnetically imaged eddy current lattices as also observed in Figure 11. Current circulation in such magnetically imaged lattices will be the same as the one moving in the corresponding copper lattices. As a consequence, the longitudinal eddy current distribution would be amplified by the neighboring ferric sheet. Nevertheless, the geometrical tissue of such magnetically imaged eddy current lattices is influenced by both skin and proximity effects as shown in Figure 11 since the current density is

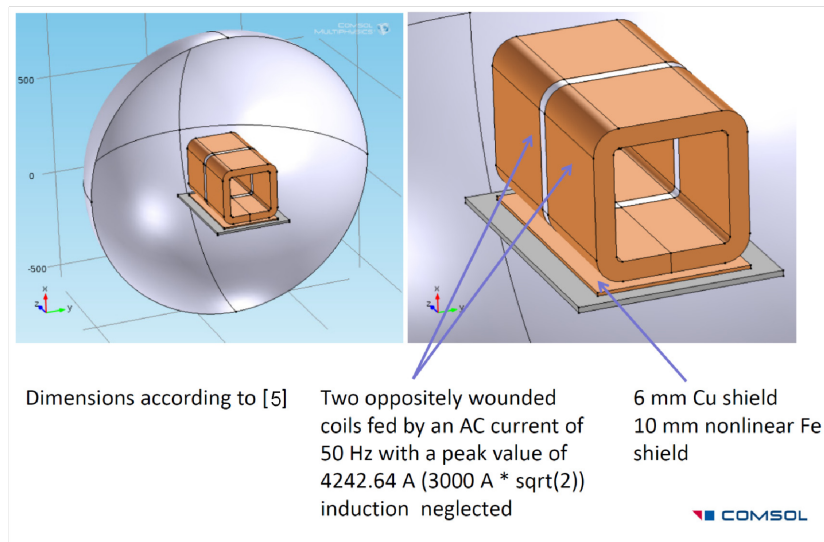


Figure 10. Benchmark No. 3 (TEAM 21): Geometry and materials of ferric plate shielded by copper screen

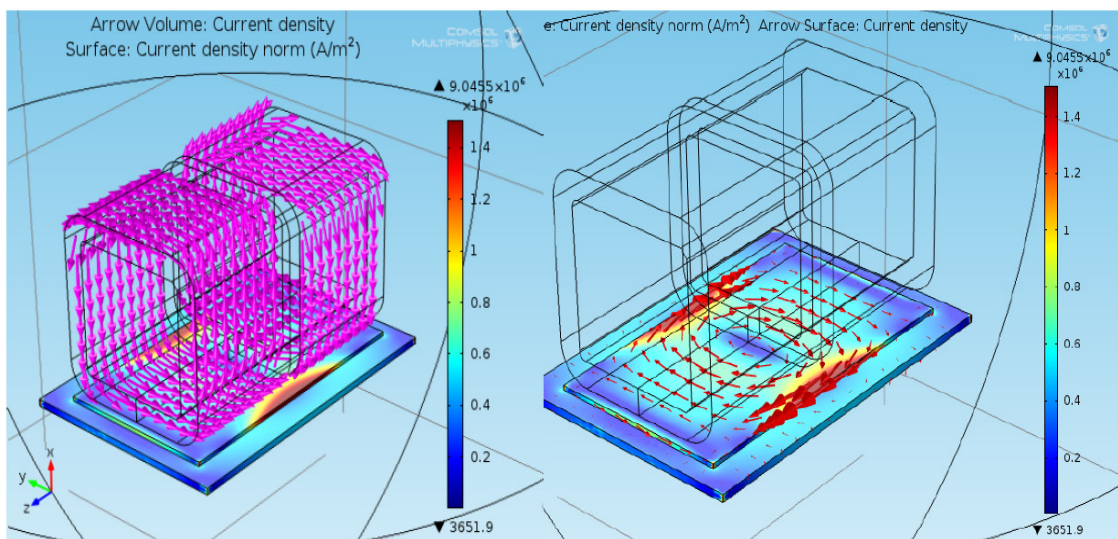


Figure 11. Benchmark No. 3 (TEAM 21): Source & Induced Current Density

exponentially decaying when moving towards the plate end. Therefore, induced eddy currents reach their peak values along the middle plane, equally splitting the shield and the plate. Such peaks are positioned on the lateral surfaces while weakening out by skin and proximity effects if moving towards the plane's centre.

The magnetic field enhancement in the nonlinear iron shield is shown on a logarithmic scale in Figure 12, while Figure 13 illustrates the power loss distribution along the shield and plate.

The logarithmic scaling indicates that the local power loss density in the iron differs by more than 5 orders of magnitude. If studying the power loss distribution within slices cut along the two plates, one notices that the contribution from the copper shield is almost a flat constant value. Such a result was expected because the skin-depth for copper is around 1 cm at 50 Hz, while the shield itself is 6 mm thick.

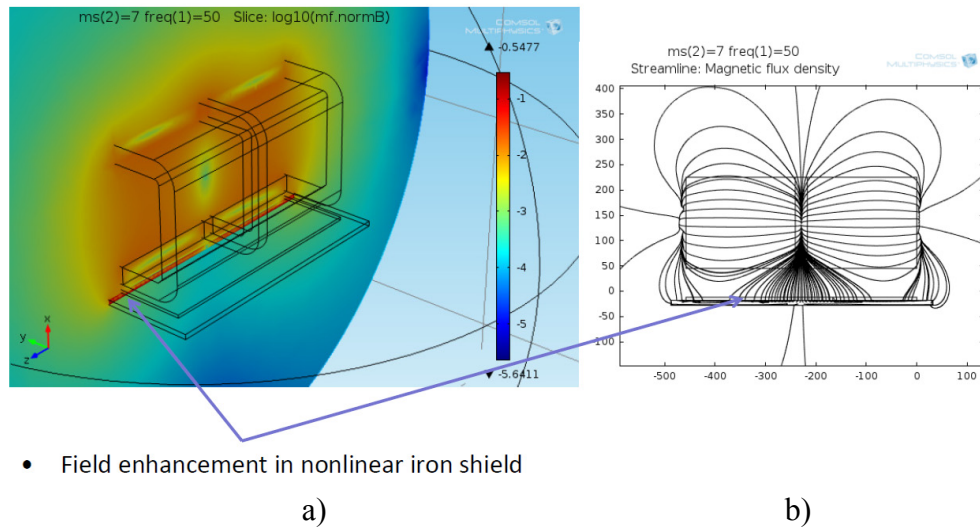


Figure 12. Benchmark No. 3 (TEAM 21): Magnetic Induction in the iron plate:
 a) Logarithmic surface plot of absolute flux density ($\log[|B|]$) at slice $y=0$
 b) xz -Streamlines of magnetic flux density at slice $y=0$

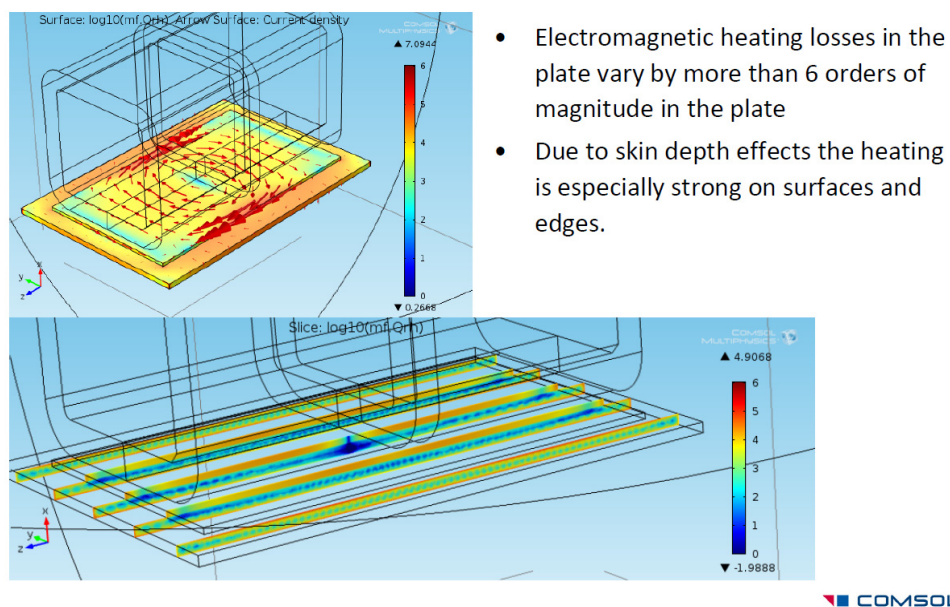


Figure 13. Benchmark No. 3 (TEAM 21): Power Losses in iron plate (logarithmic scale)

Computed copper power losses were about 11.4 Watts and did not fluctuate when increasing the mesh density from 100 thousand to about 300 thousand tetrahedral elements.

If monitoring the power loss distribution in the iron regions of the analyzed slices within Figure 13, a net skin effect is manifesting, because of iron's relatively large magnetic permeability. The colored map used in Figure 13 for the power loss distribution, is closely following these underlying physics aspects.

Iron power losses fluctuated from 8.89 Watts for the coarser mesh, up to 6.19 Watts for the finer one. The total power losses were of 20.09 Watts when using 100 thousand elements, while dropping to 17.57 Watts when using 300 thousand elements. Cheng reported in [5] a computed total power loss of 16.22 Watts, against the measured 15.24 Watts target value. The margin of error is of 15% for COMSOL results if compared against the measurement.

Perhaps the discrepancy could be explained by a linear magnetic approach used within the COMSOL harmonic solver, where no higher harmonics were considered even if iron is strongly magnetically nonlinear. Since no infinite elements were used in the COMSOL model, the magnetic field was squeezed into an unrealistic small domain and therefore, such an event could also be partially explaining the total power loss discrepancy of this preliminary study.

5. Conclusions

Three different benchmarks were selected to validate numerical results while using COMSOL against measurements and other referenced numerical solutions mentioned in the technical literature. These test problems were chosen according to relevant topics of interest for turbo-generator manufacturers. Both COMSOL Electric Currents and Magnetic solvers were used. Special features such as smart thin transition layers used for modeling interfaces with strong electromagnetic contrasts, or the default procedures used to address electric and magnetic nonlinearities, impedance boundary conditions, and even the mathematical engine capabilities to solve ill-conditioned scenarios characterized by weak electric and magnetic couplings, leading to matrices with a bad condition number, were carefully investigated.

Preliminary numerical results were encouraging and indicated that COMSOL is capable of handling such problems, which are daily business for turbo-generator R&D.

6. References

- [1] TEAM Workshop, Test Problems, 1988.
- [2] K. Fujiwara, T. Nakata, Results for Benchmark Problem 7 (Asymmetrical Conductor with a Hole), *International Journal for Computation and Mathematics in Electrical and Electronic Engineering*, Vol. 9, No. 3, pp. 137 - 154, 1993.
- [3] Y. Fujishima, S. Wakao, Surface Charge Analysis in Eddy Current Problems, *IEEE Transactions on Magnetics*, Vol. 39, No. 3, pp. 1123 - 1126, 2003.
- [4] M. Everett et al., 3-D Finite Element Analysis of Induction Logging in a Dipping Formation, *IEEE on Geoscience & Remote Sensing*, Vol. 39, No. 10, pp. 2244 - 2252, 2001.
- [5] Z. Cheng et al., Loss Spectrum and Electromagnetic Behavior of Problem 21 Family, *IEEE Transactions on Magnetics*, Vol. 42, No. 4, pp. 1467 - 1470, 2006.
- [6] M. Mailand et al., Electric Field Measurements on MV and HV components with an electro-optic sensor, 4th International Conference on Insulated Power Cables, HV Technology 15, Paris, France, 1995.

7. Acknowledgements

The authors would like to thank Dr. Atilla Banyai for his valuable assistance while formatting the paper according to the template required for publication in the COMSOL Conference Proceedings.